

1 **The Positive Effect of Formaldehyde on the Photocatalytic
2 Renoxification of Nitrate on TiO₂ Particles**

3
4 Yuhan Liu, Xuejiao Wang, Jing Shang*, Weiwei Xu, Mengshuang Sheng, Chunxiang

5 Ye

6 *State Key Joint Laboratory of Environmental Simulation and Pollution Control,*

删除[禹]: Yuhan Liu, Xuejiao Wang, Mengshuang Sheng,
Chunxiang Ye, Jing Shang*

7 *College of Environmental Sciences and Engineering, Peking University, 5 Yiheyuan*

8 *Road, Beijing 100871, P. R. China*

9

10 Corresponding author: Jing Shang

11 Email: shangjing@pku.edu.cn

12

13 **Abstract**

14 Renoxification is the process of recycling of NO₃⁻/HNO₃ into NO_x under
15 illumination, which is mostly ascribed to the photolysis of nitrate. TiO₂, a typical
16 mineral dust component, can play its photocatalytic role in “renoxification” process
17 due to NO₃ radical formed, and we define this process as “photocatalytic
18 renoxification”. Formaldehyde (HCHO), the most abundant carbonyl compound in
19 the atmosphere, may participate in the renoxification of nitrate-doped TiO₂ particles.

20 In this study, we established a 400 L environmental chamber reaction system capable | 删除[禹]: an
21 of controlling 0.8-70% relative humidity at 293K, with the presence of 1 or 9 ppm
22 HCHO and 4 wt.% nitrate-doped TiO₂. The direct photolyses of both nitrate and NO₃

23 radical were excluded by adjusting the illumination wavelength, so as to explore the
24 effect of HCHO on the “photocatalytic renoxidation”. It is found that NO_x
25 concentration can reach up to more than 100 ppb for nitrate-doped TiO_2 particles,
26 while almost no NO_x was generated in the absence of HCHO. Nitrate type, relative
27 humidity and HCHO concentration were found to influence NO_x release. It was
28 suggested that substantial amounts of NO_x were produced via the
29 NO_3^- - NO_3^\cdot - HNO_3 - NO_x pathway, where TiO_2 worked for converting “ NO_3^- ” to
30 “ NO_3^\cdot ”, HCHO participated in transformation of “ NO_3^\cdot ” to “ HNO_3 ” through
31 hydrogen abstraction, and “ HNO_3 ” photolysis answered for mass NO_x release. So,
32 HCHO played a significant role in this “photocatalytic renoxidation” process. These
33 results were found based on simplified mimics for atmospheric mineral dust under
34 specific experimental conditions, which might deviate from the real situation, but
35 illustrated a possible way of HCHO in influencing nitrate renoxidation in the
36 atmosphere. Our proposed reaction mechanism by which HCHO promotes
37 photocatalytic renoxidation is helpful for deeply understanding the atmospheric
38 photochemical processes and nitrogen cycling, and could be considered for better
39 fitting of atmospheric model simulations with field observations in some specific
40 scenarios.

删除[禹]: Adsorbed HCHO may react with nitrate radicals through hydrogen abstraction to form adsorbed HNO_3 on the surface, which is responsible for the release of NO_x . The mass generation of NO_x was suggested to via the NO_3^- - NO_3^\cdot -HCHO- HNO_3 - NO_x pathway, with HCHO and TiO_2 exhibiting a significant synergistic effect.

41 1 Introduction

42 The levels of ozone (O_3) and hydroxyl radicals ($\cdot\text{OH}$) in the troposphere can be
43 promoted by nitrogen oxides ($\text{NO}_x = \text{NO} + \text{NO}_2$), such that NO_x plays an important
44 role in the formation of secondary aerosols and atmospheric oxidants (Platt et al.,

45 1980; Stemmler et al., 2006; Harris et al., 1982; Finlayson-Pitts and Pitts, 1999). NO_x
46 can be converted into nitric acid (HNO_3) and nitrate (NO_3^-) through a series of
47 oxidation and hydrolysis reactions and is eventually removed from the atmosphere
48 through subsequent wet or dry deposition (Dentener and Crutzen, 1993; Goodman et
49 al., 2001; Monge et al., 2010; Bedjanian and El Zein, 2012). However, comparisons
50 of observations and modeling results for the marine boundary layer, land, and free
51 troposphere (Read et al., 2008; Lee et al., 2009; Seltzer et al., 2015) have shown
52 underestimation of HNO_3 or NO_3^- content, NO_x abundance, and NO_x/HNO_3 ratios,
53 indicating the presence of a new, rapid NO_x circulation pathway (Ye et al., 2016b;
54 Reed et al., 2017). Some researchers have suggested that deposited NO_3^- and HNO_3
55 can be recycled back to gas phase NO_x under illumination, via the renoxification
56 process (Schuttlefield et al., 2008; Romer et al., 2018; Bao et al., 2020; Shi et al.,
57 2021b). Photolytic renoxification occurs under light with a wavelength of < 350 nm,
58 through the photolysis of $\text{NO}_3^-/\text{HNO}_3$ adsorbed on the solid surface to generate NO_x .
59 Notably, the photolysis of $\text{NO}_3^-/\text{HNO}_3$ is reported to occur at least 2 orders of
60 magnitude faster on different solid surfaces (natural or artificial) or aerosols than in
61 the gas phase (Ye et al., 2016a; Zhou et al., 2003; Baergen and Donaldson, 2013).
62 Several recent studies have shown that renoxification has important atmospheric
63 significance (Deng et al., 2010; Kasibhatla et al., 2018; Romer et al., 2018; Alexander
64 et al., 2020), providing the atmosphere with a new source of photochemically reactive
65 nitrogen species, i.e., HONO or NO_x , resulting in the production of more
66 photooxidants such as O_3 or $\cdot\text{OH}$ (Ye et al., 2017), which further oxidize volatile

67 organic compounds (VOCs), leading to the formation of more chromophores, thereby
68 affecting the photochemical process (Bao et al., 2020).

69 Renoxification processes have recently been observed on different types of
70 atmospheric particles, such as urban grime and mineral dust (Ninneman et al., 2020;
71 Bao et al., 2018; Baergen and Donaldson, 2013; Ndour et al., 2009). Atmospheric
72 titanium dioxide (TiO_2) is mainly derived from windblown mineral dust, with mass
73 mixing ratios ranging from 0.1 to 10% (Chen et al., 2012). TiO_2 is widely used in
74 industrial processes and building exteriors for its favorable physical and chemical
75 properties. Titanium and nitrate ions have been found to coexist in atmospheric
76 particulates in different regions worldwide (Sun et al., 2005; Liu et al., 2005; Yang et
77 al., 2011; Kim et al., 2012), and the NO_3^- /(NO_3^- + TiO_2) mass percentage of total
78 suspended particulate matter (TSP) during dust storms can be lower than 20% (Sun et
79 al., 2005). In this case, nitrate-coated TiO_2 (NO_3^- - TiO_2) aerosols containing TiO_2 as
80 the main body can in some extent be used to, represent the real situation under
81 sandstorm. TiO_2 is a semiconductor metal oxide that can facilitate the photolysis of
82 nitrate and the release of NO_x due to its photocatalytic activity (Ndour et al., 2009;
83 Chen et al., 2012; Verbruggen, 2015; Schwartz-Narbonne et al., 2019). Under
84 ultraviolet (UV) light, TiO_2 generates electron-hole pairs in the conduction and
85 valence bands, respectively (Linsebigler et al., 1995). Nitrate ions adsorbed at the
86 oxide surface react with the photogenerated holes (h^+) to form nitrate radicals ($\text{NO}_3\cdot$),
87 which are subsequently photolyzed to NO_x , mainly under visible light illumination
88 (Schuttlefield et al., 2008; George et al., 2015; Schwartz-Narbonne et al., 2019). Thus,

删除[禹]: The relative content of TiO_2 and NO_3^- in atmospheric particles varies greatly

删除[禹]: and

删除[禹]: effectively

删除[禹]: represent particles for sandstorm modeling (Sun et al., 2005; Kim et al., 2012)

89 the renoxification of NO_3^- is faster on TiO_2 than on other oxides in mineral dust
90 aerosols such as SiO_2 or Al_2O_3 (Lesko et al., 2015; Ma et al., 2021). In this study, we
91 refer to renoxification involving h^+ and NO_3^- in the reaction as photocatalytic
92 renoxification based on the photocatalytic properties of TiO_2 .

93 Many previous studies have focused mainly on particulate nitrate- NO_x

94 photochemical cycling reactions, despite the potential impact of other reactant gases

95 in the atmosphere. Formaldehyde (HCHO), the most abundant carbonyl compound in

96 the atmosphere, can reach as high as 0.4 ppm in some specific situations (particularly

刪除[禹]: which can react

97 in some indoor air or cities with high traffic density) (International Agency for

98 Research on Cancer, 1995; Salthammer, 2019). HCHO can react at night with

99 NO_3^- via hydrogen abstraction reactions to form HNO_3 (Atkinson, 1991). Our

100 previous study showed that the degradation rate of HCHO was faster on NO_3^- - TiO_2

101 aerosols than on TiO_2 particles, perhaps as a result of HCHO oxidation by

102 NO_3^- (Shang et al., 2017). To date, no studies have reported the effect of HCHO on

103 photocatalytic renoxification. Adsorbed HCHO would react with NO_3^- generated on

104 the NO_3^- - TiO_2 aerosol surface, thus alter the surface nitrogenous species and

105 renoxification process. The present study is the first to explore the combined effect of

106 HCHO and photocatalytic TiO_2 particles on the renoxification of nitrate. The

107 wavelengths of the light sources were adjusted to exclude photolytic renoxification

108 while making photocatalytic renoxification available for better elucidate the reaction

109 mechanism. We investigated the effects of various influential factors including nitrate

110 type, nitrate content, RH, and initial HCHO concentration, to understand the

111 atmospheric renoxification of nitrate in greater detail.

112 **2 Methods**

113 **2.1 Environmental chamber setup**

114 Details of the experimental apparatus and protocol used in the current study have
115 been previously described (Shang et al., 2017). Briefly, the main body of the
116 environmental chamber is a 400 L polyvinyl fluoride (PVF) bag filled with synthetic
117 air (high purity N₂ (99.999%) mixed with high purity O₂ (99.999%) in the ratio of
118 79:21 by volume, Beijing Huatong Jingke Gas Chemical Co.). The chamber is
119 capable of temperature (~293 K) and relative humidity (0.8–70%) control using a
120 water bubbler and air conditioners, respectively. The chamber is equipped with two
121 light sources both with the central wavelength of 365 nm. One is a set of 36 W tube
122 lamps with a main spectrum of 320–400 nm and a small amount of 480-600 nm
123 visible light (Figure S1a). The other is a set of 12 W Light-emitting diode (LED)
124 lamps with a narrow main spectrum of 350-390 nm (Figure S1b). The light intensities
125 for the tube and LED lamp at 365 nm were 300 $\mu\text{W}\cdot\text{cm}^{-2}$ and 200 $\mu\text{W}\cdot\text{cm}^{-2}$,
126 respectively, measured in the middle of the chamber. NO_x concentrations at the outlet
127 of the chamber were monitored by a chemiluminescence NO_x analyzer (ECOTECH,
128 EC9841B). HCHO was generated by thermolysis of paraformaldehyde at 70 °C and
129 detected via acetyl acetone spectrophotometric method using a UV-Vis
130 spectrophotometer (PERSEE, T6) or a fluorescence spectrophotometer (THERMO,
131 Lumina), depending on different initial HCHO concentrations. The particle size
132 distribution was measured by a Scanning Nano Particle Spectrometer (HCT,

133 SNPS-20). Electron Spin Resonance (Nuohai Life Science, MiniScope MS 5000) was
134 used to measure ·OH on the surface of particles. 5,5-dimethyl-1-pyrroline-N-oxide
135 (DPMO, Enzo) was used as the capture agent. 50 μ L particle-containing suspension
136 mixed with 50 μ L DMPO (concentration of 200 μ M) was loaded in a 1 mm capillary.
137 Four 365 nm LED lamps were placed side by side vertically at a distance of about 1
138 cm from the capillary, and the measurement was carried out after 1 min of irradiation.
139 The modulation frequency was 100 kHz, the modulation amplitude was 0.2 mT, the
140 microwave power was 10 mW and the sweep time was 60 s.

141 **2.2 Nitrate-TiO₂ composite samples**

142 In our experiments, two nitrate salts, potassium nitrate (AR, Beijing Chemical
143 Works Co., Ltd) or ammonium nitrate (AR, Beijing Chemical Works Co., Ltd), were
144 composited, with pure TiO₂ (\geq 99.5%, Degussa AG) powder or TiO₂ (1 wt.%)/SiO₂ 删除[禹]: complexed
145 mixed powder to prepare NO₃⁻-TiO₂ or NO₃⁻-TiO₂ (1 wt.%)/SiO₂ samples. 250 mg
146 TiO₂ was simply mixed in nitrate solutions at the desired mass mixing ratio (with
147 nitrate content of 4 wt.%) to obtain a mash. The mash was dried at 90 °C and then
148 ground carefully for 30 min. A series of samples with different amount of nitrate were
149 prepared and diffuse reflectance fourier transform infrared spectroscopy (DRIFTS)
150 measurements were made to test their homogeneity. Figure S2 shows DRIFTS spectra
151 of these KNO₃-TiO₂ composites, of which 1760 cm^{-1} peak is one of the typical
152 vibrating peaks of nitrate (Aghazadeh, 2016; Maeda et al., 2011). Ratio value of peak
153 area from 1730-1790 cm^{-1} for 1, 4, 32, 80 wt.% composited samples is 1: 4.1: 29.8:
154 81.6, which is very close to that of theoretical value, proving that the samples were

155 uniformly mixed. SiO_2 (AR, Xilong Scientific Co., Ltd.) with no optical activity was
156 also chosen for comparison, and samples of $\text{KNO}_3\text{-SiO}_2$ and $\text{KNO}_3\text{-TiO}_2$ (1
157 wt.%) /SiO_2 samples with a potassium nitrate content of 4 wt.% were prepared. The
158 blank 250 mg TiO_2 sample was solved in pure water with the same procedure as
159 mentioned above. 4 wt.% $\text{HNO}_3\text{-TiO}_2$ composite particles were prepared for
160 comparison. Concentrated nitric acid (AR, Beijing Chemical Works Co., Ltd) was
161 diluted to 1 M and 250 mg TiO_2 was added to the nitric acid solution and stirred
162 evenly. A layer of aluminum foil was covered on the surface of the $\text{HNO}_3\text{-TiO}_2$
163 homogenate and dried naturally in the room and then ground for use. We also selected
164 Arizona Test Dust (ATD, Powder Technology Inc.), whose chemical composition and
165 weight percentage were shown in Table S1, as a substitute of $\text{NO}_3^-/\text{TiO}_2$ to investigate
166 the “photocatalytic renoxification” process of nitrate and the positive effect of HCHO .

167 **2.3 Environmental chamber experiments**

168 For the chamber operation, we completely evacuated the chamber after every
169 experiment, then cleaned the chamber walls with deionized water and then dried by
170 flushing the chamber with ultra-zero air to remove any particles or gases collected on
171 the chamber walls. The experiments carried out in the environmental chamber can be
172 divided into two categories according to whether HCHO was involved or not. (1) No
173 HCHO involvement in the reaction. The PVF bag was inflated by 260 L synthetic air,
174 and then 75 mg particles were instantly sprayed into the chamber by a transient
175 high-pressure airflow. As shown in Figure S3, the particle number concentration of
176 $\text{KNO}_3\text{-TiO}_2$ or TiO_2 sample decreased rapidly owing to wall effect including the

177 possible electrostatic adsorption of the particles by the environmental chamber. The
178 size distributions of $\text{KNO}_3\text{-TiO}_2$ and TiO_2 samples were similar, with both reached
179 stable after about 60 min. The peak number concentration was averaged of 3991 and
180 3886 particle/cm³ during illumination period for $\text{KNO}_3\text{-TiO}_2$ and TiO_2 sample,
181 respectively, indicating that the repeatability of the introduction of particles into the
182 chamber is good. This can be attributed to the strict cleaning of the chamber and the
183 same operation of each batch experiment. (2) With the participation of HCHO. The
184 PVF bag was inflated by 125 L synthetic air, followed by the introduction of HCHO,
185 and then the chamber was filled up with zero air to about 250 L. In order to know the
186 HCHO adsorption before and after the particles' introduction, we conducted a
187 conditional experiment in the dark. It can be seen from Figure S4 that it took about 90
188 min for the concentration of HCHO to reach stable, and can be sustained. Then, 75
189 mg TiO_2 or $\text{NO}_3^-/\text{TiO}_2$ powders were introduced instantly and the concentration of
190 HCHO decreased upon the introduction. It took about 60 min for HCHO to reach its
191 second adsorption equilibrium, and the concentration of HCHO can be stable for
192 several hours in the dark. Therefore, for the irradiation experiments, the particles were
193 injected at 90 min after HCHO's introduction, and the lamps were turned on at 60 min
194 after the particle's introduction.

195 To determine the background value of NO_x in the reaction system, four blank
196 experiments were carried out under illumination without nitrate: "synthetic air",
197 "synthetic air + TiO_2 ", "synthetic air + HCHO" and "synthetic air + HCHO + TiO_2 ".
198 In the blank experiments of "synthetic air" and "synthetic air + TiO_2 ", the NO_x

199 concentration remained stable during 180 min illumination, and the concentration
200 change was no more than 0.5 ppb (Figure S5a). Therefore, the environmental chamber,
201 synthetic air and the surface of TiO₂ particles were thought to be relatively clean, and
202 there was no generation and accumulation of NO_x under illumination. When HCHO
203 was introduced into the environmental chamber, NO_x accumulated ~2 ppb in 120 min
204 with or without TiO₂ particles (Figure S5b). Compared with the blank experiment
205 results when there was no HCHO, NO_x might come from the generation process of
206 HCHO (impurities in paraformaldehyde). However, considering the high
207 concentration level of NO_x produced in the NO₃⁻-TiO₂ system containing HCHO
208 under the same conditions in this study (see later in Figure 2), the NO_x generated in
209 this blank experiment can be negligible.

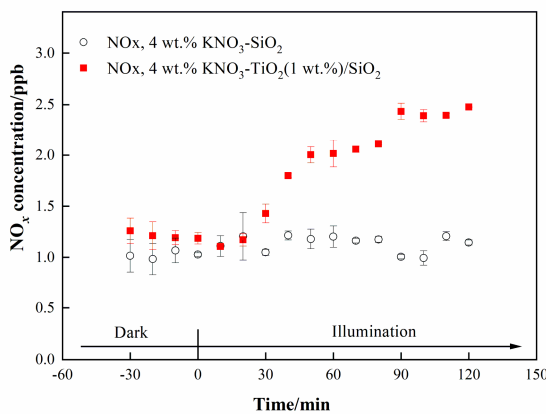
210

211 **3 Results and discussion**

212 **3.1 The positive effect of TiO₂ on the renoxidation process**

213 We investigated the photocatalytic role of TiO₂ on renoxidation. The light
214 source was two 365 nm tube lamps containing small amounts of 400–600 nm visible
215 light; this setup was suitable for exciting TiO₂ and the photolysis of available nitrate
216 radicals. Raw NO_x data measured in the chamber under dark and illuminated
217 conditions for 4 wt.% KNO₃-SiO₂ and 4 wt.% KNO₃-TiO₂ (1 wt.-%)/SiO₂ are shown
218 in Figure 1. The ratio of 1 wt. % TiO₂ to SiO₂ corresponds to their ratio in sand and
219 dust particles. We observed no NO_x in the KNO₃-SiO₂ sample under dark or
220 illumination, indicating very weak direct photolysis of nitrate under our 365 nm

221 tube-lamp illumination conditions. However, when the sample containing $\text{TiO}_2/\text{SiO}_2$
222 was illuminated, NO_x continually accumulated in the chamber. This finding confirms
223 that NO_x production arising from photodissociation of NO_3^- on $\text{TiO}_2/\text{SiO}_2$ was caused
224 by the photocatalytic property of TiO_2 (i.e., photocatalytic renoxidation) and was not
225 due to the direct photolysis of NO_3^- (photolytic renoxidation).

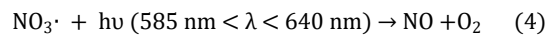
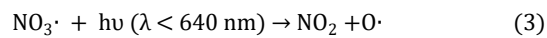
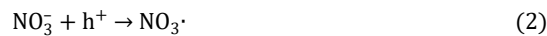
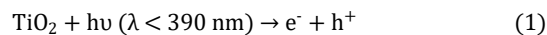


226
227 **Figure 1.** Effect of illumination on the release of NO_x from 4 wt.% $\text{KNO}_3\text{-SiO}_2$ and 4
228 wt.% $\text{KNO}_3\text{-TiO}_2(1 \text{ wt.}\%) \text{/SiO}_2$ at 293 K and 0.8% of relative humidity. 365 nm tube
229 lamps were used during the illumination experiments.

230 TiO_2 can be excited by UV illumination to generate electron-hole pairs, and the
231 h^+ can react with adsorbed NO_3^- to produce $\text{NO}_3\cdot$ (Ndour et al., 2009). Thus, in the
232 present study, $\text{NO}_3\cdot$ mainly absorbed visible light emitted from the tube lamps, which
233 was subsequently photolyzed to NO_x through Eqs. (3) and (4) (Wayne et al., 1991),
234 which explains why NO_x was observed in this study. Thus, we demonstrated that TiO_2
235 can be excited at illumination wavelengths of $\sim 365 \text{ nm}$, even when the content was
236 very low, and that NO_x accumulated due to the production and further photolysis of

刪除[禹]: y

237 NO_3^\cdot . However, the production rate of NO_x was very slow, reaching only 1.3 ppb
238 during 90 min of illumination. This result may have been caused by the blocking
239 effect of K^+ on NO_3^- . K^+ forms ion pairs with NO_3^- , and electrostatic repulsion
240 between K^+ and h^+ prevents NO_3^- from combining with h^+ to generate NO_3^\cdot to a
241 certain extent, thereby weakening the positive effect of TiO_2 on the renoxidation of
242 KNO_3 (Rosseler et al., 2013).



243

244

245 **3.2 The synergistic positive effect of TiO_2 and HCHO on the renoxidation
246 process**

247 LED lamps with a wavelength range of 350–390 nm and no visible light were
248 used to irradiate 4 wt.% $\text{KNO}_3\text{-TiO}_2$ without generating NO_x (NO_2 and NO
249 concentrations fluctuate within the error range of the instrument) (Figure S5). TiO_2
250 can be excited under this range of irradiation, producing NO_3^\cdot radicals as discussed
251 above. The lack of NO_x generation indicates that neither nitrate photolysis nor
252 NO_3^\cdot photolysis occurred under 365 nm LED lamp illumination conditions. In
253 addition, it has been shown that NO_3^\cdot photolysis only occurs in visible light (Aldener
254 et al., 2006). Therefore, the LED lamp setup was used in subsequent experiments to

255 exclude the direct photolysis of both KNO_3 and NO_3^\cdot , but allow the excitation of TiO_2 .
256 This approach allowed us to investigate the process of photocatalytic renoxidation
257 caused by HCHO in the presence of photogenerated NO_3^\cdot .

258 Atmospheric trace gases can undergo photocatalytic reactions on the surface of
259 TiO_2 (Chen et al., 2012). As the illumination time increased, the concentration of
260 HCHO showed a linear downward trend, which was found to fit zero-order reaction
261 kinetics (Figure S7). The zero-order reaction rate constants of HCHO on TiO_2 and 4
262 wt.% KNO_3 - TiO_2 particles were 9.1×10^{-3} and 1.4×10^{-2} ppm min^{-1} , respectively,
263 which were much higher than that for gaseous HCHO photolysis (Shang et al., 2017).

264 We suggested that the produced NO_3^\cdot contributed to the enhanced uptake of HCHO.
265 In the following study, the effect of HCHO on the photocatalytic renoxidation of
266 NO_3^\cdot - TiO_2 was explored.

267 Variation in NO_x concentration within the chamber containing nitrate- TiO_2
268 particles with or without HCHO is shown in Figure 2. For 4 wt.% KNO_3 - TiO_2
269 particles, the NO_x concentration began to increase upon irradiation in the presence of
270 HCHO, reaching ~ 3861 mmol-normalized ppb (equivalent to 110 ppb) within 120
271 min. This result indicates that HCHO greatly promoted photocatalytic renoxidation
272 of KNO_3 on the surfaces of TiO_2 particles. This reaction process can be divided into
273 two stages: a rapid increase within the first 60 min and a slower increase within the
274 following 60 min, each consistent with zero-order reaction kinetics. The slow stage is
275 due to the photodegradation of HCHO on KNO_3 - TiO_2 aerosols, which led to a
276 decrease in its concentration, gradually weakening the positive effect. NO_x is the sum

277 of NO_2 and NO , both of which showed a two-stage concentration increase (Figure S8).

278 The NO_2 generation rate was nearly 6 times that of NO , as compared to using the

279 zero-order rate constant within 60 min ($1.18 \text{ ppb min}^{-1} \text{ NO}_2$, $R^2 = 0.96$; 0.19 ppb

280 $\text{min}^{-1} \text{ NO}$, $R^2 = 0.91$). This burst-like generation of NO_x can be ascribed to the

281 reaction between generated $\text{NO}_3\cdot$ and HCHO via hydrogen abstraction to form

282 adsorbed nitric acid ($\text{HNO}_3(\text{ads})$) on TiO_2 particles. We measured the pH of water

283 extracts in NO_3^- - TiO_2 systems with and without HCHO . It was found that the pH

284 decreased by 1.7% for KNO_3 - TiO_2 , suggesting the formation of acidic species such as

285 $\text{HNO}_3(\text{ads})$ in this study. Based on the analysis of the absorption cross section of

286 HNO_3 adsorbed on fused silica surface, the $\text{HNO}_3(\text{ads})$ absorption spectrum has been

287 reported to be red-shifted compared to $\text{HNO}_3(\text{g})$, extending from 350 to 365 nm, with

288 a simultaneous cross-sectional increase (Du and Zhu, 2011). Therefore, $\text{HNO}_3(\text{ads})$

289 was subjected to photolysis to produce NO_2 and HONO (Eqs. (6)-(8)) under the LED

290 lamp used in this study. A previous study of HNO_3 photolysis on the surface of Pyrex

291 glass showed that the ratio of the formation rates of photolysis products

292 ($J_{\text{NO}_x}/J_{(\text{NO}_x+\text{HONO})}$) was $> 97\%$ at $\text{RH} = 0\%$ (Zhou et al., 2003), suggesting that NO_x is

293 the main gaseous product under dry conditions. Thus, the effect of HONO on product

294 distribution and NO_x concentration was negligible in this study. Together, these results

295 suggest that $\text{NO}_3\cdot$ and HCHO generate $\text{HNO}_3(\text{ads})$ on particle surfaces through

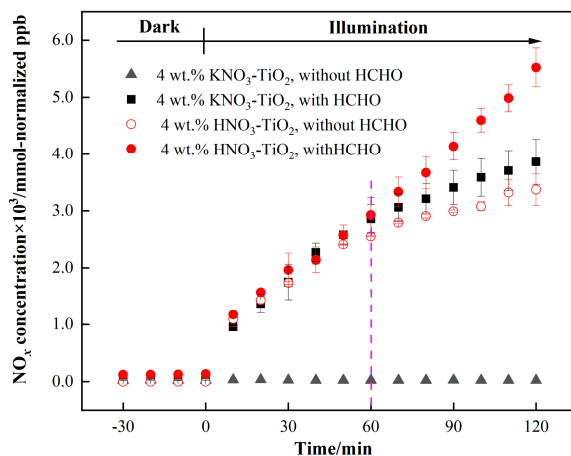
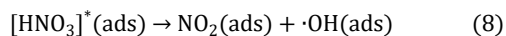
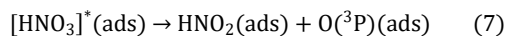
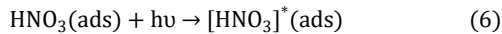
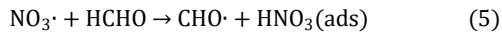
296 hydrogen abstraction, which contributes to the substantial release of NO_x via

297 photolysis. This photocatalytic renoxidation via the NO_3^- - $\text{NO}_3\cdot$ - HNO_3 - NO_x pathway

刪除[禹]: - HCHO

298 is important considering the high abundance of hydrogen donor organics in the

299 atmosphere.



300

301 **Figure 2.** Effect of formaldehyde on the renoxidation processes of different nitrate-

302 doped particles at 293 K and 0.8% of relative humidity. 365 nm LED lamps were used

303 during the illumination experiment. The initial concentration of HCHO was about 9

304 ppm.

305 To demonstrate the proposed HCHO mechanism and the photolysis contribution

306 of HNO₃ to NO_x, we prepared an HNO₃-TiO₂ sample by directly dissolving TiO₂ into

307 dilute nitric acid. The formation of NO_x on HNO₃-TiO₂ without HCHO under

308 illumination was obvious and at a rate comparable with that on KNO₃-TiO₂ with

309 HCHO (Figure 2). The renoxidation of HNO₃-TiO₂ particles was further enhanced

310 following the introduction of HCHO. This is because that HNO_3 dissociates on
311 particle surfaces to generate NO_3^- , such that HNO_3 exists on TiO_2 as both $\text{HNO}_3(\text{ads})$
312 and $\text{NO}_3^-(\text{ads})$. Similarly, $\text{NO}_3^-(\text{ads})$ completed the $\text{NO}_3^- \rightarrow \text{NO}_3 \cdot \rightarrow \text{HNO}_3 \rightarrow \text{NO}_x$ pathway | 刪除[禹]: -HCHO
313 as described above through the reaction process shown in Eqs. (2) to (8). The rates of
314 NO_x production from $\text{HNO}_3\text{-TiO}_2$ particles with and without HCHO were similar for
315 the first 60 min (Figure 2), mainly due to the direct photolysis of partial $\text{HNO}_3(\text{ads})$.
316 However, after 60 min, NO_x was generated rapidly in the presence of HCHO, perhaps
317 due to the dominant photocatalytic renoxidation of $\text{NO}_3^-(\text{ads})$. These findings
318 indicate that HCHO converts NO_3^- on particle surfaces into $\text{HNO}_3(\text{ads})$ by reacting
319 with $\text{NO}_3 \cdot$, and then $\text{HNO}_3(\text{ads})$ photolyses at a faster rate to generate NO_x , allowing
320 HCHO to enhance the formation of NO_x . Overall, the photocatalytic renoxidation of
321 $\text{NO}_3^-\text{-TiO}_2$ particles affects atmospheric oxidation and the nitrogen cycle, and the
322 presence of HCHO further enhances this impact.

323 Photocatalytic renoxidation reaction occurs on the surfaces of mineral dust due
324 to the presence of semiconductor oxides with photocatalytic activity such as TiO_2
325 (Ndour et al., 2009). In order to confirm this, we synthesized nitrate with inert SiO_2 as
326 a comparison. It can be seen from Figure S9 that no NO_2 formation was observed
327 whether HCHO was present or not, indicating that photocatalytically active particle
328 TiO_2 is critical to the photocatalytic renoxidation process. Furthermore, a kind of
329 commercial mineral dust ATD was selected to study the effects of HCHO on this
330 process. We detected $\cdot\text{OH}$ in irradiated pure TiO_2 and ATD samples using electron
331 spin resonance (ESR) technique, and found that for ATD samples, the peak intensity

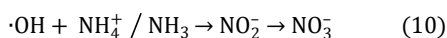
332 of ·OH generation was 40% that of TiO₂ samples (Figure S10). ·OH originates in the
333 reaction of h⁺ with surface adsorbed water (Ahmed et al., 2014). ATD contains
334 semiconductor oxides such as TiO₂ and Fe₂O₃, and is thought to exhibit photocatalytic
335 properties affecting the renoxidation of nitrate. The NO₃⁻ content of ATD is 4 × 10¹⁷
336 molecules m⁻², which is ~0.25 wt.% of the total mass (Huang et al., 2015; Jiyeon et
337 al., 2017). The NO_x concentration changes observed in the environmental chamber
338 demonstrated that HCHO promoted the renoxidation of ATD particles (Figure S11).
339 This result suggests that mineral dust containing photocatalytic semiconductor oxides
340 such as TiO₂, Fe₂O₃, and ZnO can greatly promote the conversion of granular nitrate
341 to NO_x in the presence of HCHO.

342 **3.3 Influential factors on the photocatalytic renoxidation process**

343 **3.3.1 The influence of nitrate type**

344 As discussed above, HNO₃ and KNO₃ undergo different renoxidation processes
345 on the surface of TiO₂ under the same illumination conditions, suggesting that cations
346 bound to NO₃⁻ significantly affect NO_x production. Different types of cations coexist
347 with nitrate ions in atmospheric particulate matter, among which ammonium ions
348 (NH₄⁺) are important water-soluble ions that can be higher in content than K⁺ in urban
349 fine particulate matter (Zhou et al., 2016; Tang et al., 2021; Wang et al., 2021),
350 especially in heavily polluted cities.(Tian et al., 2020) Equal amounts of 4 wt.%
351 NH₄NO₃-TiO₂ particles were introduced into the chamber and illuminated under the
352 same conditions. Similar as Figure 2, millimole normalized ppb was used in order to
353 compare the amount of NO_x release for different kinds of nitrate with same percentage

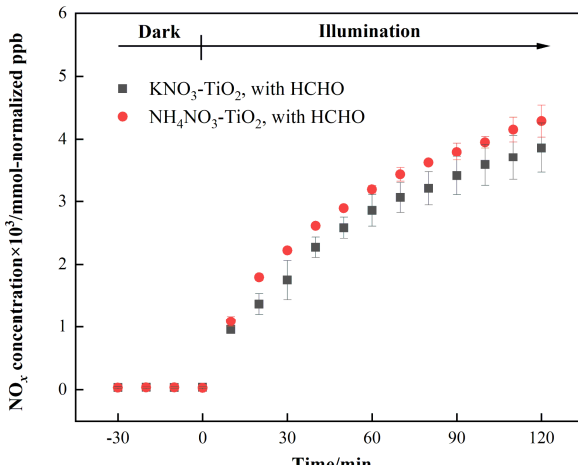
354 weight. It can be seen that HCHO had a much stronger positive effect on the release
355 of NO_x over $\text{NH}_4\text{NO}_3\text{-TiO}_2$ particles (Figure 3), which may be ascribed to NH_4^+ .
356 Combined with the results of $\text{NH}_4\text{NO}_3\text{-TiO}_2$ and $\text{KNO}_3\text{-TiO}_2$ particles, it seems that
357 the affinity rather than electrostatic repulsion should be the primary effect of cations
358 on the production of NO_x . On substrates without photocatalytic activity such as SiO_2
359 and Al_2O_3 , NH_4NO_3 cannot generate NO_x , such that NO_x production depends on the
360 effect of TiO_2 (Ma et al., 2021). The h^+ generated by TiO_2 excitation reacts with
361 adsorbed H_2O to produce $\cdot\text{OH}$ (Eq. (9)), which gradually oxidizes NH_4^+ to NO_3^- (Eq.
362 (10)). In our previous study, we demonstrated that irradiated $(\text{NH}_4)_2\text{SO}_4\text{-TiO}_2$ samples
363 had lower NH_4^+ and NO_3^- peaks (Shang et al., 2017). Therefore, more NO_3^-
364 participated in the photocatalytic renoxification process via the
365 NO_3^- - $\text{NO}_3\cdot$ - HNO_3 - NO_x pathway to generate NO_x . Moreover, the results without
366 HCHO are shown in Figure S12, both $\text{NH}_4\text{NO}_3\text{-TiO}_2$ particles and $\text{KNO}_3\text{-TiO}_2$
367 particles produced almost no NO_x , indicating the importance of HCHO for
368 renoxification to occur. Due to the high content of NH_4NO_3 in atmospheric particulate
369 matter, the positive effect of HCHO on the photocatalytic renoxification process may
370 have some impact on the concentrations of NO_x and other atmospheric oxidants.



刪除[禹]: such that NO_x production depends on the effect of TiO_2

刪除[禹]: - HCHO

刪除[禹]: ,



372

373 **Figure 3.** Effect of formaldehyde on the renoxidation processes of 4 wt.%

374 NH₄NO₃-TiO₂ and 4 wt.% KNO₃-TiO₂ particles at 293 K and 0.8% of relative

375 humidity. 365 nm LED lamps were used during the irradiation experiment. The initial

376 concentration of HCHO was about 9 ppm.

377

378 **3.3.2 The influence of relative humidity**

379 Water on particle surfaces can participate directly in the heterogeneous reaction

380 process. As shown in Eq. (9), H₂O can be captured by h⁺ to generate ·OH with strong

381 oxidizability in photocatalytic reactions. The first-order photolysis rate constant of

382 NO₃⁻ on TiO₂ particles decreases by an order of magnitude, from $(5.7 \pm 0.1) \times 10^{-4} \text{ s}^{-1}$

383 on dry surfaces to $(7.1 \pm 0.8) \times 10^{-5} \text{ s}^{-1}$ when nitrate is coadsorbed with water above

384 monolayer coverage (Ostaszewski et al., 2018). We explored the positive effect of

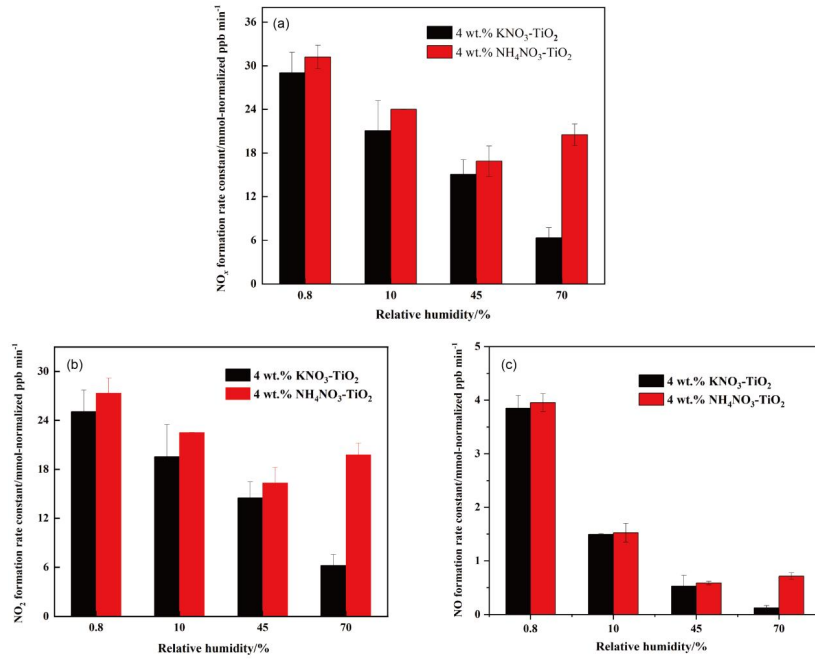
385 HCHO on the NO₃⁻-TiO₂ particle photocatalytic renoxidation at different RH levels;

386 the results are shown in Figure 4a. For KNO₃-TiO₂ particles, the rate of NO_x

387 production decreased as the RH of the environmental chamber increased, indicating
388 that increased water content in the gas phase hindered photocatalytic renoxidation
389 for two reasons: H_2O competes with NO_3^- for h^+ on the surface of TiO_2 to | 删除[禹]: i
390 generate $\cdot\text{OH}$, reducing the generation of $\text{NO}_3\cdot$, and competitive adsorption between
391 H_2O and HCHO causes the generated $\cdot\text{OH}$ to compete with $\text{NO}_3\cdot$ for HCHO ,
392 hindering the formation of $\text{HNO}_3(\text{ads})$ on particle surfaces. Moreover, it is also
393 possible that the loss of NO_x on the wall increases under high humidity conditions,
394 resulting in a decrease in its concentration. This competitive process also occurs on
395 the surface of $\text{NH}_4\text{NO}_3\text{-TiO}_2$ particles, but at $\text{RH} = 70\%$, the NO_x generation rate
396 constant is slightly higher. The deliquescent humidity of NH_4NO_3 at 298 K is $\sim 62\%$,
397 such that NH_4NO_3 had already deliquesced at $\text{RH} = 70\%$, forming an $\text{NH}_4^+/\text{NH}_3\text{-NO}_3^-$
398 liquid system on the particle surfaces. This quasi-liquid phase improved the dispersion
399 of TiO_2 in NH_4NO_3 , resulting in greater NO_x release. The deliquescent humidity of
400 $\text{KNO}_3\text{-TiO}_2$ was $> 90\%$, (2009) such that no phase change occurred at $\text{RH} = 70\%$, and
401 the renoxidation reaction rate retained a downward trend. In the presence of H_2O , in
402 addition to the NO_3^- - $\text{NO}_3\cdot$ - HNO_3 pathway observed in this study, there are a variety | 删除[禹]: - HCHO
403 of HNO_3 generation paths, such as the hydrolysis of N_2O_5 via the $\text{NO}_2\text{-N}_2\text{O}_5\text{-HNO}_3$
404 pathway (Brown et al., 2005), the oxidation of NO_2 by $\cdot\text{OH}$ (Burkholder et al., 1993),
405 and the reaction of $\text{NO}_3\cdot$ with H_2O (Schutze and Herrmann, 2005), all of which
406 require further consideration and study.

407 The formation rates of NO and NO_2 are shown in Figure 4b and c, respectively.
408 NO_2 was the main product of surface HNO_3 photolysis. Under humid conditions,

409 generated $\text{NO}_2(\text{ads})$ continued to react with H_2O adsorbed on the surface to form
410 $\text{HONO}(\text{ads})$. HONO was desorbed from the surface and released into the gas phase
411 (Zhou et al., 2003; Bao et al., 2018; Pandit et al., 2021), providing gaseous HONO to
412 the reaction system. Because the NO_x concentration remained high, the effect of
413 HONO on NO_x analyzer results was negligible (Shi et al., 2021a). As NO_2 can form
414 NO_2^- with e^- , a reverse reaction also occurred between NO_2^- and HONO in the
415 presence of H_2O (Ma et al., 2021; Garcia et al., 2021). Therefore, the increase in H_2O
416 increased the proportion of HONO in the nitrogen-containing products, such that the
417 NO_x generation rate decreased as RH increased. Comparing Figure 4b and c shows
418 that, as RH increased, the NO production rate constant decreased more than that of
419 NO_2 . HONO and NO_2 generated by the photolysis of $\text{HNO}_3(\text{ads})$ decreased
420 accordingly, i.e., the NO source decreased. However, generated NO_2 and NO
421 underwent photocatalytic oxidation on the surface of TiO_2 , and NO photodegradation
422 was more significant under the same conditions (Hot et al., 2017). Generally, a certain
423 amount of HONO will be generated during the reaction between HCHO and
424 NO_3^- - TiO_2 particles when RH is high, which affects the concentrations of
425 atmospheric $\cdot\text{OH}$, NO_x , and O_3 . This process is more likely to occur in summer due to
426 high RH and light intensity affecting atmospheric oxidation. In drier winters or dusty
427 weather, when TiO_2 content is high, HCHO greatly promotes the photocatalytic
428 renoxidation of NO_3^- - TiO_2 particles, thereby releasing more NO_x into the atmosphere,
429 affecting the global atmospheric nitrogen budget. Thus, regardless of the seasonal and
430 regional changes, renoxidation has significant practical importance.



431

432 **Figure 4.** Effect of relative humidity on the release of NO_x (a), NO_2 (b), NO (c) over 4

433 wt.% $\text{NH}_4\text{NO}_3\text{-TiO}_2$ and 4 wt.% $\text{KNO}_3\text{-TiO}_2$ particles at 293 K. 365 nm LED lamps

434 were used during the illumination experiment. The initial concentration of HCHO was

435 about 9 ppm.

436

437 **3.3.3 The influence of initial HCHO concentration**

438 To explore whether HCHO promotes nitrate renoxification at natural

439 concentration levels, we reduced the initial concentration of HCHO in the

440 environmental chamber by a factor of 10, to ~1.0 ppm. The positive effect of HCHO

441 on the photocatalytic renoxification of $\text{KNO}_3\text{-TiO}_2$ particles was clearly weakened,

442 with NO_2 concentration first increasing and then decreasing, and NO concentration

刪除[禹]: 5

443 remaining stable (Figure S13). The HCHO concentration decreased due to its
444 consumption during the reaction, making its positive effect decline quickly. The
445 photocatalytic oxidation reaction between NO_x and photogenerated reactive oxygen
446 species (ROS) on the TiO_2 surface further decreased the NO_x concentration.
447 Photocatalytic oxidation of NO_x by ROS on TiO_2 particles occurred at an HCHO
448 concentration of 9 ppm, but the positive effect of HCHO remained dominant. Thus,
449 no decrease in NO_x concentration was observed within 120 min in our experiments.

450 The concentration of HCHO in the atmosphere is relatively low, with a balance
451 between the photocatalytic oxidation decay of NO_x and the release of NO_x via
452 photocatalytic renoxification. The mutual transformation between particulate NO_3^-
453 and gaseous NO_x is more complex. The effect of low-concentration HCHO on the
454 renoxification of NO_3^- - TiO_2 particles requires further investigation. However, many
455 types of organics provide hydrogen atoms in the atmosphere, including alkanes (e.g.,
456 methane and n-hexane), aldehydes (e.g., acetaldehyde), alcohols (e.g., methanol and
457 ethanol), and aromatic compounds (e.g., phenol) that react with $\text{NO}_3\cdot$ to produce nitric
458 acid (Atkinson, 1991). These organics, together with HCHO, play similar positive
459 roles in photocatalytic renoxification and, therefore, influence NO_x concentrations.

460

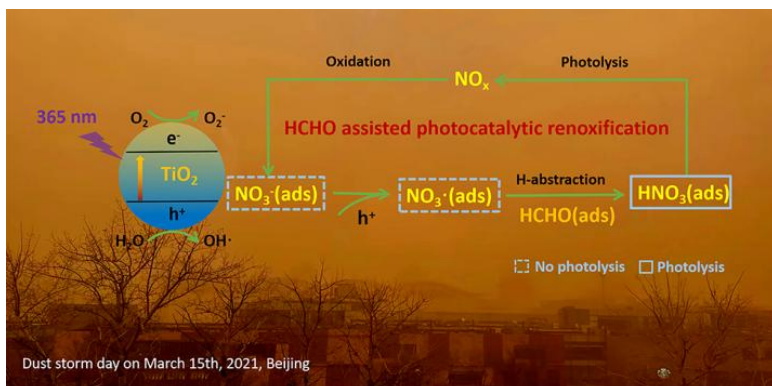
461 **4 Atmospheric implications**

462 Nitric acid and nitrate are not only the final sink of NO_x in the atmosphere but
463 are also among its important sources. NO_x from nitrate through renoxification is easily
464 overlooked. The renoxification of nitrate on the surface of TiO_2 particles can be

465 divided into photolytic renoxification and photocatalytic renoxification. The
466 photocatalytic performance of TiO_2 promotes the renoxification process, which
467 explains the influence of semiconducting metal oxide components on atmospheric
468 mineral particles during the renoxification of nitrate. Although most previous studies
469 have focused on solid-phase nitrate renoxification, our exploration of the roles of
470 HCHO in this study will allow us to examine complex real-world pollution scenarios,
471 in which multiple atmospheric pollutants coexist, as well as the effects of organic
472 pollutants on the renoxification process. Atmospheric HCHO is taken up at the
473 surface of particulate matter, accounting for up to ~50% of its absorption (Li et al.,
474 2014), such that the heterogeneous participation of HCHO during renoxification is
475 important. This study is the first to report that HCHO has a positive effect on the
476 photocatalytic renoxification of nitrate on TiO_2 particles, via the
477 NO_3^- - $\text{NO}_3\cdot$ - HNO_3 - NO_x pathway (Figure 5), further increasing the release of NO_x and
478 other nitrogen-containing active species, which in turn affects the photochemical
479 cycle of HO_x radicals in the atmosphere and the formation of important atmospheric
480 oxidants such as O_3 . Although in the case of high concentrations of HCHO in our
481 experiment, the response to the real situation will be biased, the results of this study
482 illustrate a possible way of HCHO in influencing nitrate renoxification in the
483 atmosphere. Factors such as particulate matter composition, RH, and initial HCHO
484 concentration all influence the positive effect of HCHO; notably, H_2O competes with
485 NO_3^- for photogenerated holes. Based on these findings, two balance systems should
486 be explored in depth: the influence of RH on the generation rates of HONO and NO_x ,

刪除[禹]: - HCHO

487 as water increases the proportion of HONO in nitrogen-containing products; and the
488 balance between the photocatalytic degradation of generated NO_x on TiO_2 particles
489 and the positive effect of HCHO on NO_x generation at low HCHO concentrations.



490
491 **Figure 5.** Positive role of HCHO on the photocatalytic renoxidation of nitrate- TiO_2
492 composite particles via the NO_3^- - NO_3^\cdot - HNO_3 - NO_x pathway. | 删除[禹]: -HCHO

493 Based on our results, we conclude that in photochemical processes on the
494 surfaces of particles containing semiconductor oxides, with the participation of
495 hydrogen donor organics, a significant synergistic photocatalytic renoxidation
496 enhancement effect could alter the composition of surface nitrogenous species via the
497 NO_3^- - NO_3^\cdot - HNO_3 - NO_x pathway, thereby affecting atmospheric oxidation and
498 nitrogen cycling. The positive effect of HCHO can be extended from TiO_2 in this
499 study to other components of mineral dust such as Fe_2O_3 and ZnO with photocatalytic
500 activity, which may have practical applications. Our proposed reaction mechanism by
501 which HCHO promotes photocatalytic renoxidation could improve existing
502 atmospheric chemistry models and reduce discrepancies between model simulations
503 and field observations.

504

505 ***Supplement.***

506 Detailed information of Figures S1-13 (which include the spectra of the lamps,
507 size distribution of 4 wt.% $\text{KNO}_3\text{-TiO}_2$ and TiO_2 particles and changes of HCHO
508 concentration in environmental chamber, changes of NO_x concentration under
509 different reaction conditions, photodegradation curve of HCHO , ESR spectra of TiO_2
510 and ATD particles), and Table S1 (which demonstrate ATD chemical composition).

刪除[禹]:

511

512 ***Acknowledgments***

513 The authors are grateful to the financial support provided by National Natural
514 Science Foundation of China (Nos. 21876003, 41961134034 and 21277004), the
515 Second Tibetan Plateau Scientific Expedition and Research (No. 2019QZKK0607).

516

517 ***References***

518 Aghazadeh, M.: Preparation of Gd_2O_3 Ultrafine Nanoparticles by Pulse
519 Electrodeposition Followed by Heat-treatment Method, Journal of Ultrafine Grained
520 and Nanostructured Materials, 49, 80-86, 10.7508/jufgnsm.2016.02.04, 2016.
521 Ahmed, A. Y., Kandiel, T. A., Ivanova, I., and Bahnemann, D.: Photocatalytic and
522 photoelectrochemical oxidation mechanisms of methanol on TiO_2 in aqueous solution,
523 Applied Surface Science, 319, 44-49, 10.1016/j.apsusc.2014.07.134, 2014.
524 Aldener, M., Brown, S. S., Stark, H., Williams, E. J., Lerner, B. M., Kuster, W. C.,
525 Goldan, P. D., Quinn, P. K., Bates, T. S., Fehsenfeld, F. C., and Ravishankara, A. R.:
526 Reactivity and loss mechanisms of NO_3 and N_2O_5 in a polluted marine environment:
527 Results from in situ measurements during New England Air Quality Study 2002,

528 Journal of Geophysical Research-Atmospheres, 111, D23S73, 10.1029/2006jd007252,
529 2006.

530 Alexander, B., Sherwen, T., Holmes, C. D., Fisher, J. A., Chen, Q., Evans, M. J., and
531 Kasibhatla, P.: Global inorganic nitrate production mechanisms: comparison of a
532 global model with nitrate isotope observations, Atmospheric Chemistry and Physics,
533 20, 3859-3877, 10.5194/acp-20-3859-2020, 2020.

534 Atkinson, R.: Kinetics and mechanisms of the gas-phase reactions of the NO_3 radical
535 with organic-compounds, Journal of Physical and Chemical Reference Data, 20,
536 459-507, 10.1063/1.555887, 1991.

537 Baergen, A. M. and Donaldson, D. J.: Photochemical Renoxification of Nitric Acid on
538 Real Urban Grime, Environmental Science & Technology, 47, 815-820,
539 10.1021/es3037862, 2013.

540 Bao, F., Li, M., Zhang, Y., Chen, C., and Zhao, J.: Photochemical Aging of Beijing
541 Urban $\text{PM}_{2.5}$: HONO Production, Environmental Science & Technology, 52,
542 6309-6316, 10.1021/acs.est.8b00538, 2018.

543 Bao, F., Jiang, H., Zhang, Y., Li, M., Ye, C., Wang, W., Ge, M., Chen, C., and Zhao, J.:
544 The Key Role of Sulfate in the Photochemical Renoxification on Real $\text{PM}_{2.5}$,
545 Environmental Science & Technology, 54, 3121-3128, 10.1021/acs.est.9b06764,
546 2020.

547 Bedjanian, Y. and El Zein, A.: Interaction of NO_2 with TiO_2 Surface Under UV
548 Irradiation: Products Study, Journal of Physical Chemistry A, 116, 1758-1764,
549 10.1021/jp210078b, 2012.

550 Brown, S. S., Osthoff, H. D., Stark, H., Dube, W. P., Ryerson, T. B., Warneke, C., de
551 Gouw, J. A., Wollny, A. G., Parrish, D. D., Fehsenfeld, F. C., and Ravishankara, A. R.:
552 Aircraft observations of daytime NO_3 and N_2O_5 and their implications for
553 tropospheric chemistry, Journal of Photochemistry and Photobiology a-Chemistry,
554 176, 270-278, 10.1016/j.jphotochem.2005.10.004, 2005.

555 Burkholder, J. B., Talukdar, R. K., Ravishankara, A. R., and Solomon, S.:
556 Temperature-dependence of the HNO_3 UV absorption cross-sections, Journal of
557 Geophysical Research-Atmospheres, 98, 22937-22948, 10.1029/93jd02178, 1993.

558 Chen, H., Nanayakkara, C. E., and Grassian, V. H.: Titanium Dioxide Photocatalysis
559 in Atmospheric Chemistry, Chemical Reviews, 112, 5919-5948, 10.1021/cr3002092,
560 2012.

561 Deng, J. J., Wang, T. J., Liu, L., and Jiang, F.: Modeling heterogeneous chemical
562 processes on aerosol surface, Particuology, 8, 308-318, 10.1016/j.partic.2009.12.003,
563 2010.

564 Dentener, F. J. and Crutzen, P. J.: Reaction of N_2O_5 on tropospheric aerosols-impact
565 on the global distributions od NO_x , O_3 , and OH , Journal of Geophysical
566 Research-Atmospheres, 98, 7149-7163, 10.1029/92jd02979, 1993.

567 Du, J. and Zhu, L.: Quantification of the absorption cross sections of surface-adsorbed
568 nitric acid in the 335-365 nm region by Brewster angle cavity ring-down spectroscopy,
569 Chemical Physics Letters, 511, 213-218, 10.1016/j.cplett.2011.06.062, 2011.

570 Finlayson-Pitts, B. J. and Pitts, J. J. N.: Chemistry of the Upper and Lower
571 Atmosphere: Theory, Experiments and Applications, 10.1023/A:1024719803484,
572 Academic Press1999.

573 Garcia, S. L. M., Pandit, S., Navea, J. G., and Grassian, V. H.: Nitrous Acid (HONO)
574 Formation from the Irradiation of Aqueous Nitrate Solutions in the Presence of
575 Marine Chromophoric Dissolved Organic Matter: Comparison to Other Organic
576 Photosensitizers, Acs Earth and Space Chemistry, 5, 3056-3064,
577 10.1021/acsearthspacechem.1c00292, 2021.

578 George, C., Ammann, M., D'Anna, B., Donaldson, D. J., and Nizkorodov, S. A.:
579 Heterogeneous Photochemistry in the Atmosphere, Chemical Reviews, 115,
580 4218-4258, 10.1021/cr500648z, 2015.

581 Goodman, A. L., Bernard, E. T., and Grassian, V. H.: Spectroscopic study of nitric
582 acid and water adsorption on oxide particles: Enhanced nitric acid uptake kinetics in
583 the presence of adsorbed water, Journal of Physical Chemistry A, 105, 6443-6457,
584 10.1021/jp0037221, 2001.

585 Harris, G. W., Carter, W. P. L., Winer, A. M., Pitts, J. N., Platt, U., and Perner, D.:
586 Observations of nitrous-acid in the los-angeles atmosphere and implications for

587 predictions of ozone precursor relationships, Environmental Science & Technology,
588 16, 414-419, 10.1021/es00101a009, 1982.

589 Hot, J., Martinez, T., Wayser, B., Ringot, E., and Bertron, A.: Photocatalytic
590 degradation of NO/NO₂ gas injected into a 10 m³ experimental chamber,
591 Environmental Science and Pollution Research, 24, 12562-12570,
592 10.1007/s11356-016-7701-2, 2017.

593 Huang, L., Zhao, Y., Li, H., and Chen, Z.: Kinetics of Heterogeneous Reaction of
594 Sulfur Dioxide on Authentic Mineral Dust: Effects of Relative Humidity and
595 Hydrogen Peroxide, Environmental Science & Technology, 49, 10797-10805,
596 10.1021/acs.est.5b03930, 2015.

597 International Agency for Research on Cancer: Wood Dust and formaldehyde, IARC
598 Monographs on the Evaluation of the Carcinogenic Risk of Chemicals to Humans, 62
599 10.1007/BF00054167, 1995.

600 Jiyeon, Park, Myoseon, Jang, Zechen, and Yu: Heterogeneous Photo-oxidation of SO₂
601 in the Presence of Two Different Mineral Dust Particles: Gobi and Arizona Dust,
602 Environmental Science & Technology, 51, 9605-9613, 10.1021/acs.est.7b00588,
603 2017.

604 Kasibhatla, P., Sherwen, T., Evans, M. J., Carpenter, L. J., Reed, C., Alexander, B.,
605 Chen, Q., Sulprizio, M. P., Lee, J. D., Read, K. A., Bloss, W., Crilley, L. R., Keene, W.
606 C., Pszenny, A. A. P., and Hodzic, A.: Global impact of nitrate photolysis in sea-salt
607 aerosol on NO_x, OH, and O₃ in the marine boundary layer, Atmospheric Chemistry
608 and Physics, 18, 11185-11203, 10.5194/acp-18-11185-2018, 2018.

609 Kim, W.-H., Song, J.-M., Ko, H.-J., Kim, J. S., Lee, J. H., and Kang, C.-H.:
610 Comparison of Chemical Compositions of Size-segregated Atmospheric Aerosols
611 between Asian Dust and Non-Asian Dust Periods at Background Area of Korea,
612 Bulletin of the Korean Chemical Society, 33, 3651-3656,
613 10.5012/bkcs.2012.33.11.3651, 2012.

614 Lee, J. D., Moller, S. J., Read, K. A., Lewis, A. C., Mendes, L., and Carpenter, L. J.:
615 Year-round measurements of nitrogen oxides and ozone in the tropical North Atlantic

616 marine boundary layer, *Journal of Geophysical Research-Atmospheres*, 114, D21302,
617 10.1029/2009jd011878, 2009.

618 Lesko, D. M. B., Coddens, E. M., Swomley, H. D., Welch, R. M., Borgatta, J., and
619 Navea, J. G.: Photochemistry of nitrate chemisorbed on various metal oxide surfaces,
620 *Physical Chemistry Chemical Physics*, 17, 20775-20785, 10.1039/c5cp02903a, 2015.

621 Li, X., Rohrer, F., Brauers, T., Hofzumahaus, A., Lu, K., Shao, M., Zhang, Y. H., and
622 Wahner, A.: Modeling of HCHO and CHOCHO at a semi-rural site in southern China
623 during the PRIDE-PRD2006 campaign, *Atmospheric Chemistry and Physics*, 14,
624 12291-12305, 10.5194/acp-14-12291-2014, 2014.

625 Linsebigler, A. L., Lu, G. Q., and Yates, J. T.: Photocatalysis on TiO_2
626 surfaces-principles, mechanisms, and selected results, *Chemical Reviews*, 95,
627 735-758, 10.1021/cr00035a013, 1995.

628 Liu, W., Wang, Y. H., Russell, A., and Edgerton, E. S.: Atmospheric aerosol over two
629 urban-rural pairs in the southeastern United States: Chemical composition and
630 possible sources, *Atmospheric Environment*, 39, 4453-4470,
631 10.1016/j.atmosenv.2005.03.048, 2005.

632 Ma, Q., Zhong, C., Ma, J., Ye, C., Zhao, Y., Liu, Y., Zhang, P., Chen, T., Liu, C., Chu,
633 B., and He, H.: Comprehensive Study about the Photolysis of Nitrates on Mineral
634 Oxides, *Environmental Science & Technology*, 55, 8604-8612,
635 10.1021/acs.est.1c02182, 2021.

636 Maeda, N., Urakawa, A., Sharma, R., and Baiker, A.: Influence of Ba precursor on
637 structural and catalytic properties of Pt-Ba/alumina NO_x storage-reduction catalyst,
638 *Applied Catalysis B-Environmental*, 103, 154-162, 10.1016/j.apcatb.2011.01.022,
639 2011.

640 Monge, M. E., D'Anna, B., and George, C.: Nitrogen dioxide removal and nitrous
641 acid formation on titanium oxide surfaces--an air quality remediation process?,
642 *Physical Chemistry Chemical Physics*, 12, 8991-8998, 10.1039/b925785c, 2010.

643 Ndour, M., Conchon, P., D'Anna, B., Ka, O., and George, C.: Photochemistry of
644 mineral dust surface as a potential atmospheric renoxidation process, *Geophysical
645 Research Letters*, 36, 4, 10.1029/2008gl036662, 2009.

646 Ninneman, M., Lu, S., Zhou, X. L., and Schwab, J.: On the Importance of
647 Surface-Enhanced Renoxification as an Oxides of Nitrogen Source in Rural and
648 Urban New York State, *Acs Earth and Space Chemistry*, 4, 1985-1992,
649 10.1021/acsearthspacechem.0c00185, 2020.

650 Ostaszewski, C. J., Stuart, N. M., Lesko, D. M. B., Kim, D., Lueckheide, M. J., and
651 Navea, J. G.: Effects of Coadsorbed Water on the Heterogeneous Photochemistry of
652 Nitrates Adsorbed on TiO₂, *Journal of Physical Chemistry A*, 122, 6360-6371,
653 10.1021/acs.jpca.8b04979, 2018.

654 Pandit, S., Garcia, S. L. M., and Grassian, V. H.: HONO Production from Gypsum
655 Surfaces Following Exposure to NO₂ and HNO₃: Roles of Relative Humidity and
656 Light Source, *Environmental Science & Technology*, 55, 9761-9772,
657 10.1021/acs.est.1c01359, 2021.

658 Platt, U., Perner, D., Harris, G. W., Winer, A. M., and Pitts, J. N.: Observations of
659 nitrous-acid in an urban atmosphere by differential optical-absorption, *Nature*, 285,
660 312-314, 10.1038/285312a0, 1980.

661 Read, K. A., Mahajan, A. S., Carpenter, L. J., Evans, M. J., Faria, B. V. E., Heard, D.
662 E., Hopkins, J. R., Lee, J. D., Moller, S. J., Lewis, A. C., Mendes, L., McQuaid, J. B.,
663 Oetjen, H., Saiz-Lopez, A., Pilling, M. J., and Plane, J. M. C.: Extensive
664 halogen-mediated ozone destruction over the tropical Atlantic Ocean, *Nature*, 453,
665 1232-1235, 10.1038/nature07035, 2008.

666 Reed, C., Evans, M. J., Crilley, L. R., Bloss, W. J., Sherwen, T., Read, K. A., Lee, J.
667 D., and Carpenter, L. J.: Evidence for renoxification in the tropical marine boundary
668 layer, *Atmospheric Chemistry and Physics*, 17, 4081-4092,
669 10.5194/acp-17-4081-2017, 2017.

670 Romer, P. S., Wooldridge, P. J., Crounse, J. D., Kim, M. J., Wennberg, P. O., Dibb, J.
671 E., Scheuer, E., Blake, D. R., Meinardi, S., Brosius, A. L., Thames, A. B., Miller, D.
672 O., Brune, W. H., Hall, S. R., Ryerson, T. B., and Cohen, R. C.: Constraints on
673 Aerosol Nitrate Photolysis as a Potential Source of HONO and NO_x, *Environmental
674 Science & Technology*, 52, 13738-13746, 10.1021/acs.est.8b03861, 2018.

675 Rosseler, O., Sleiman, M., Nahuel Montesinos, V., Shavorskiy, A., Keller, V., Keller,
676 N., Litter, M. I., Bluhm, H., Salmeron, M., and Destaillats, H.: Chemistry of NO_x on
677 TiO₂ Surfaces Studied by Ambient Pressure XPS: Products, Effect of UV Irradiation,
678 Water, and Coadsorbed K⁺, *Journal of Physical Chemistry Letters*, 4, 536-541,
679 10.1021/jz302119g, 2013.

680 Salthammer, T.: Formaldehyde sources, formaldehyde concentrations and air
681 exchange rates in European housings, *Building and Environment*, 150, 219-232,
682 10.1016/j.buildenv.2018.12.042, 2019.

683 Shuttlefield, J., Rubasinghege, G., El-Maazawi, M., Bone, J., and Grassian, V. H.:
684 Photochemistry of adsorbed nitrate, *Journal of the American Chemical Society*, 130,
685 12210-12211, 10.1021/ja802342m, 2008.

686 Schutze, M. and Herrmann, H.: Uptake of the NO₃ radical on aqueous surfaces,
687 *Journal of Atmospheric Chemistry*, 52, 1-18, 10.1007/s10874-005-6153-8, 2005.

688 Schwartz-Narbonne, H., Jones, S. H., and Donaldson, D. J.: Indoor Lighting Releases
689 Gas Phase Nitrogen Oxides from Indoor Painted Surfaces, *Environmental Science &*
690 *Technology Letters*, 6, 92-97, 10.1021/acs.estlett.8b00685, 2019.

691 Seltzer, K. M., Vizuete, W., and Henderson, B. H.: Evaluation of updated nitric acid
692 chemistry on ozone precursors and radiative effects, *Atmospheric Chemistry and*
693 *Physics*, 15, 5973-5986, 10.5194/acp-15-5973-2015, 2015.

694 Shang, J., Xu, W. W., Ye, C. X., George, C., and Zhu, T.: Synergistic effect of
695 nitrate-doped TiO₂ aerosols on the fast photochemical oxidation of formaldehyde,
696 *Scientific Reports*, 7, 1161, 10.1038/s41598-017-01396-x, 2017.

697 Shi, Q., Tao, Y., Krechmer, J. E., Heald, C. L., Murphy, J. G., Kroll, J. H., and Ye, Q.:
698 Laboratory Investigation of Renoxification from the Photolysis of Inorganic
699 Particulate Nitrate, *Environmental science & technology*, 55, 854-861,
700 10.1021/acs.est.0c06049, 2021.

701 Stemmler, K., Ammann, M., Donders, C., Kleffmann, J., and George, C.:
702 Photosensitized reduction of nitrogen dioxide on humic acid as a source of nitrous
703 acid, *Nature*, 440, 195-198, 10.1038/nature04603, 2006.

704 Sun, Y. L., Zhuang, G. S., Wang, Y., Zhao, X. J., Li, J., Wang, Z. F., and An, Z. S.:
705 Chemical composition of dust storms in Beijing and implications for the mixing of
706 mineral aerosol with pollution aerosol on the pathway, *Journal of Geophysical*
707 *Research-Atmospheres*, 110, D24209, 10.1029/2005jd006054, 2005.

708 Tang, M., Liu, Y., He, J., Wang, Z., Wu, Z., and Ji, D.: In situ continuous hourly
709 observations of wintertime nitrate, sulfate and ammonium in a megacity in the North
710 China plain from 2014 to 2019: Temporal variation, chemical formation and regional
711 transport, *Chemosphere*, 262, 10.1016/j.chemosphere.2020.127745, 2021.

712 Tian, S. S., Liu, Y. Y., Wang, J., Wang, J., Hou, L. J., Lv, B., Wang, X. H., Zhao, X. Y.,
713 Yang, W., Geng, C. M., Han, B., and Bai, Z. P.: Chemical Compositions and Source
714 Analysis of PM_{2.5} during Autumn and Winter in a Heavily Polluted City in China,
715 *Atmosphere*, 11, 19, 10.3390/atmos11040336, 2020.

716 Verbruggen, S. W.: TiO₂ photocatalysis for the degradation of pollutants in gas phase:
717 From morphological design to plasmonic enhancement, *Journal of Photochemistry*
718 and *Photobiology C-Photochemistry Reviews*, 24, 64-82,
719 10.1016/j.jphotochemrev.2015.07.001, 2015.

720 Wang, H., Miao, Q., Shen, L., Yang, Q., Wu, Y., Wei, H., Yin, Y., Zhao, T., Zhu, B.,
721 and Lu, W.: Characterization of the aerosol chemical composition during the
722 COVID-19 lockdown period in Suzhou in the Yangtze River Delta, China, *Journal of*
723 *environmental sciences (China)*, 102, 110-122, 10.1016/j.jes.2020.09.019, 2021.

724 Wayne, R. P., Barnes, I., Biggs, P., Burrows, J. P., Canosamas, C. E., Hjorth, J., Lebras,
725 G., Moortgat, G. K., Perner, D., Poulet, G., Restelli, G., and Sidebottom, H.: The
726 nitrate radical-physics, chemistry, and the atmosphere, *Atmospheric Environment Part*
727 *a-General Topics*, 25, 1-203, 10.1016/0960-1686(91)90192-a, 1991.

728 Yang, F., Tan, J., Zhao, Q., Du, Z., He, K., Ma, Y., Duan, F., Chen, G., and Zhao, Q.:
729 Characteristics of PM_{2.5} speciation in representative megacities and across China,
730 *Atmospheric Chemistry and Physics*, 11, 5207-5219, 10.5194/acp-11-5207-2011,
731 2011.

732 Ye, C., Gao, H., Zhang, N., and Zhou, X.: Photolysis of Nitric Acid and Nitrate on
733 Natural and Artificial Surfaces, Environmental Science & Technology, 50, 3530-3536,
734 10.1021/acs.est.5b05032, 2016a.

735 Ye, C., Zhang, N., Gao, H., and Zhou, X.: Photolysis of Particulate Nitrate as a Source
736 of HONO and NO_x, Environmental Science & Technology, 51, 6849-6856,
737 10.1021/acs.est.7b00387, 2017.

738 Ye, C., Zhou, X., Pu, D., Stutz, J., Festa, J., Spolaor, M., Tsai, C., Cantrell, C.,
739 Mauldin, R. L., III, Campos, T., Weinheimer, A., Hornbrook, R. S., Apel, E. C.,
740 Guenther, A., Kaser, L., Yuan, B., Karl, T., Haggerty, J., Hall, S., Ullmann, K., Smith,
741 J. N., Ortega, J., and Knote, C.: Rapid cycling of reactive nitrogen in the marine
742 boundary layer, Nature, 532, 489-491, 10.1038/nature17195, 2016b.

743 Zhou, J. B., Xing, Z. Y., Deng, J. J., and Du, K.: Characterizing and sourcing ambient
744 PM_{2.5} over key emission regions in China I: Water-soluble ions and carbonaceous
745 fractions, Atmospheric Environment, 135, 20-30, 10.1016/j.atmosenv.2016.03.054,
746 2016.

747 Zhou, X. L., Gao, H. L., He, Y., Huang, G., Bertman, S. B., Civerolo, K., and Schwab,
748 J.: Nitric acid photolysis on surfaces in low-NO_x environments: Significant
749 atmospheric implications, Geophysical Research Letters, 30, 2217,
750 10.1029/2003gl018620, 2003.